Gaps in the yrast level structure of the $N = 50$ isotones ^{93}Tc, ^{94}Ru, and ^{95}Rh at high angular momentum

H. A. Roth, S. E. Arnell, D. Foltescu, and Ö. Skeppstedt
Department of Physics, Chalmers University of Technology, and The University of Gothenburg, S-412 96 Göteborg, Sweden

J. Blomqvist
Department of Physics, Frescati, The Royal Institute of Technology, S-104 05 Stockholm, Sweden

A. Nilsson
The Manne Siegbahn Laboratory, The University of Stockholm, S-104 05 Stockholm, Sweden

T. Kuroyanagi and S.Mitarai
Department of Physics, Kyushu University, Hakozaki, Fukuoka, 812 Japan

J. Nyberg
Niels Bohr Institute, DK-4000 Roskilde, Denmark and The Svedberg Laboratory, Uppsala University, S-751 21 Uppsala, Sweden

(Received 28 March 1994)

The projectile-target system ^{40}Ca+^{58}Ni has been used to produce the neutron deficient $N = 50$ isotones ^{93}Tc, ^{94}Ru, and ^{95}Rh at high angular momentum. The multidetector array NORDBALL including particle selection was used. A large number of new levels were found in all three nuclei. Most of them can be interpreted as states with a neutron particle-hole excitation across the $N = 50$ shell gap, coupled to lower valence-proton configurations. Some of the observed levels above 11 MeV probably correspond to states with two neutrons excited across the shell gap.

PACS number(s): 23.20.Lv, 25.70.Jj, 21.60.Cs, 27.60.+j

I. INTRODUCTION

The N=50 isotones have, since the early days of the shell model, attracted theorists and experimentalists. A large number of calculations have been performed, from Talmi and Unna [1], in 1960, Cohen *et al.* [2], Auerbach and Talmi [3], Vervier [4], Ball *et al.* [5,7], Gloeckner *et al.* [6,8], Chiang *et al.* [9], Amusa and Lawson [10], Blomqvist and Rydström [12], Ji and Wildenthal [13], to the recent work by Sinatkas *et al.* [14]. All these calculations have assumed an inert neutron core, and calculated states formed by protons moving in the $p_{1/2}$, $g_{9/2}$ or $f_{5/2}$, $p_{3/2}$, $p_{1/2}$, $g_{9/2}$ shells.

A calculation of high-spin states assuming single-neutron excitation to the $d_{5/2}$ shell above the gap was performed by Muto *et al.* [11]. The calculation was used in comparisons with experimental high-spin states in ^{94}Ru with tentative spin assignments $J^\pi = 17$ [15] and 19^+ [16], values which are above the maximum spin values of 15^+ and 15^- obtainable in the $f_{5/2}$, $p_{3/2}$, $p_{1/2}$, $g_{9/2}$ basis (Table I). The calculation fairly well reproduced some of the positive-parity high-spin states observed [16].

Making use of recent advances in γ-ray spectroscopy combining multidetector systems of "ball" structure with exit channel selection we have investigated the yrast structure of ^{93}Tc, ^{94}Ru, and ^{95}Rh up to very high angular momenta using NORDBALL with particle channel selection [17]. The aim of the investigation is to interpret the high-spin yrast structure by shell-model configurations, thus facilitating the choice of a restricted configuration space to be used for calculations. The investigation also gives the possibility to compare the experimental structure with recent calculations using a model restricted to $p_{1/2}$, $p_{3/2}$, $f_{5/2}$, $g_{9/2}$ configurations and a ^{100}Sn core [14].

Up to the present work the following experimental information was available on the N=50 isotones mentioned above: Grecescu *et al.* [18] used the ^{92}Mo(α,2pn) reaction in a study of ^{93}Tc and reported an yrast sequence up to a $\frac{25}{2}^+$ state. Brown *et al.* [19] found a $\frac{17}{2}^-$ isomeric state using the ^{90}Zr(^{6}Li,3n) reaction. Quite recently Ghugre *et al.* [20] published a level scheme of ^{93}Tc

TABLE I. Maximum-spin values attainable for N=50 isotones. It has been assumed that the configurations involve at most one proton hole in $f_{5/2}$, $p_{3/2}$ or one neutron particle in $d_{5/2}$.

Nucleus	Configuration space		
N=50	$(p_{1/2}, g_{9/2})$	$(f_{5/2}, p_{3/2}, p_{1/2}, g_{9/2})$	$(p_{1/2}, g_{9/2}, d_{5/2})$
$^{93}_{43}$Tc	$\frac{25}{2}^+$	$\frac{31}{2}^+$	$\frac{39}{2}^+$
	$\frac{25}{2}^-$	$\frac{29}{2}^-$	$\frac{39}{2}^-$
$^{94}_{44}$Ru	12^+	15^+	19^+
	13^-	15^-	20^-
$^{95}_{45}$Rh	$\frac{25}{2}^+$	$\frac{27}{2}^+$	$\frac{39}{2}^+$
	$\frac{25}{2}^-$	$\frac{29}{2}^-$	$\frac{39}{2}^-$

with spins up to $\frac{39}{2}^+$ and $\frac{43}{2}^-$.

High-spin states of ^{94}Ru have been studied up to spin (8^+) by the $(\alpha,2n)$ reaction [21], up to (17) by Nolte *et al.* [15] by the ^{40}Ca+^{58}Ni reaction, and up to (19^+) by Piel *et al.* [16] using the ^{40}Ca+^{60}Ni reaction.

The ^{40}Ca+^{58}Ni reaction was also used by Nolte *et al.* [15] in a study of high-spin states in ^{95}Rh. Levels with spin values up to $\frac{27}{2}^+$ and $\frac{25}{2}^-$ were proposed.

II. EXPERIMENTAL PROCEDURES

The nuclei ^{93}Tc, ^{94}Ru, and ^{95}Rh were produced by the ^{40}Ca+^{58}Ni reaction at $E(^{40}\text{Ca})=180$ MeV using a stacked target consisting of three self-supporting foils with a thickness of 0.33 mg/cm^2 each (^{58}Ni enrichment 99.7%). The thin foils were at 0.21-mm distance from each other, and were followed by a beam catcher 20-mm downstream. The Doppler shift corrections were based on the value $\beta = v/c=3.7\%$. About 55×10^6 events were recorded of which, according to a CASCADE calculation [22], 73 mb of the total cross section of 760 mb ($l_{\max} \approx 56\hbar$) constituted the $5p$ reaction channel leading to ^{93}Tc, 37 mb the $4p$ channel leading to ^{94}Ru, and 1 mb the $3p$ channel leading to ^{95}Rh. In another experiment the same nuclei were produced at $E(^{40}\text{Ca})=187$ MeV using a 10 mg/cm^2 ^{58}Ni target. About 60×10^6 events were recorded. A short (1×10^6 events) run at $E(^{40}\text{Ca})=147$ MeV increased the relative contribution of ^{95}Rh (cross section 30 mb) which facilitated the analysis of this nucleus.

The particle beams, having intensities of the order of 1 particle nA, were delivered by the tandem booster accelerator at NBI, Risø, Denmark. The γ rays were detected in 15 BGO-shielded HPGe detectors situated in three rings of the NORDBALL frame [23] at 79°, 101°, and 143° relative to the beam direction. The detectors were energy and efficiency calibrated with ^{56}Co, ^{152}Eu, and ^{133}Ba sources.

The present investigation was performed at high projectile energy in order to enhance high-spin states and to get large yields from a number of residual nuclei of interest for the present investigation. This means that we had to use a very efficient particle selection system in order to detect the large number of outgoing particle combinations (21 exit channels with cross sections $\geq$1 mb). Such a system [17,24] was developed for the NORDBALL detection system in a collaboration between Kyushu University, Japan [25] and Chalmers University of Technology, Sweden [26]. In the present setup the system was adapted for spectroscopy of nuclei far from stability in the following way: In the forward hemisphere 11 liquid scintillator detectors formed a "neutron wall" [26]. For this setup the total neutron efficiency was $\varepsilon_n \approx 0.25$. Evaporated protons and α particles were detected by a 4π Si ball consisting of 21 detectors, the total efficiency values were $\varepsilon_p=0.80$ and $\varepsilon_\alpha=0.65$ as quoted by Kuroyanagi *et al.* [25]. At least two Compton suppressed γ rays had to be detected within ~100 ns in the Ge detectors together with at least one charged particle in the Si ball in order to generate a valid trigger and subsequently readout and store the events on 8-mm EXABYTE tapes. The γ-ray energy range covered is from 40 to 4000 keV.

A more detailed account of the selection of reaction channels was given in a preceding article [24] treating the yrast level structure of the $N=49$ isotones ^{92}Tc, ^{93}Ru, ^{94}Rh, and ^{95}Pd.

III. DATA REDUCTION AND EXPERIMENTAL RESULTS

The general procedure of finding a clean $\gamma\gamma$-coincidence matrix for a certain residual nucleus starts by setting a gate in the particle identification spectrum (Fig. 1) for the channel in question with the neutron condition included, if appropriate. The "raw" matrix so obtained is corrected for "leaks" from reaction channels with larger particle multiplicities. These leaks are mainly due to the limited solid angle of the particle detectors. The raw matrix is cleaned by subtracting appropriate fractions of the matrices gated by larger number of detected particles. This requires a good knowledge of the projected spectra from all channels of higher multiplic-

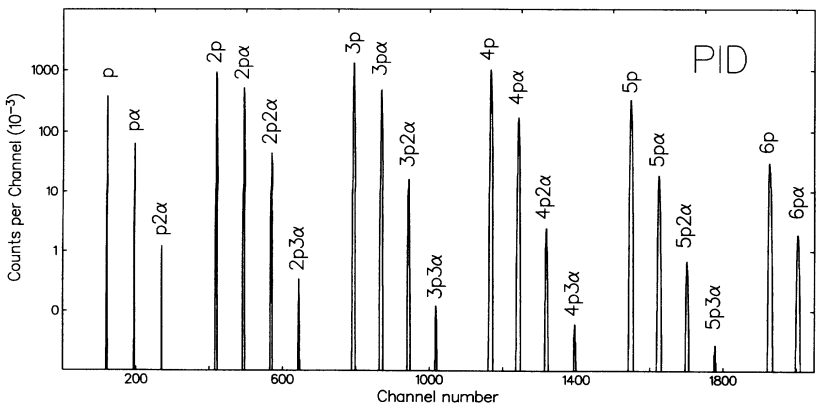

FIG. 1. Particle identification spectrum from the reaction ^{40}Ca+^{58}Ni at $E(^{40}\text{Ca})=180$ MeV. The spectrum is gated by a twofold $\gamma\gamma$ coincidence.

ity. The subtraction procedure is performed by a trial and error method.

The "raw" $\gamma\gamma$-coincidence matrices obtained by sorting all events associated with $5p(^{93}\mathrm{Tc})$, $4p(^{94}\mathrm{Ru})$, and $3p(^{95}\mathrm{Rh})$ emissions were corrected for contributions from reaction channels of higher proton multiplicities, from contributing xpn channels, as well as channels containing one or two α particles.

In the construction of the level schemes, the γ rays were placed in the scheme by use of $\gamma\gamma$-coincidence relations and γ-ray intensities. Primarily, the intensities were obtained by summing the gain-shifted and efficiency corrected contributions from the rings at 101° and 143°. The angles of the rings happen to be such as to justify this procedure irrespective of the A_2 coefficient of the angular distribution (the A_4 coefficient is negligible in this context). The computer program ESCL8R [27] was used for control of the level schemes. This program allows fast and easy inspection and fitting of the peaks in the $\gamma\gamma$-coincidence matrix and is used to construct coincidence spectra based on assumed decay patterns, which are then compared to the observed spectra. In this way the program works backwards from the proposed level scheme, and attempts to reproduce the observed $\gamma\gamma$-coincidence matrix. Information on the γ-ray anisotropies was extracted from projected spectra recorded at 79°, 101°, and 143° with respect to the beam axis. The assignment of level spins was mostly based on these anisotropies, defined as $R = 2I(143°)/[I(79°) + I(101°)]$. Considering the high angular momentum brought into the compound system, we assumed that essentially all observed transitions have $J_i \geq J_f$ and most transitions have $J_i > J_f$. Crossover transitions are generally expected to be of $E2$ character. The R values are obtained from the thick target run except for a few high-energy transitions as noted in the tables.

The use of a thin target, followed by a beam stopper, makes measurements possible of lifetimes in the region 0.1–10 ns, simply by taking the ratio between the areas of the in-flight peak and the stopped peak from the 143° ring projection. A correction for the deorientation effect can be obtained by analyzing also one of the rings at 79° and 101°. When feeding times can be neglected this method should be as good as the standard recoil distance Doppler-shift method.

A. Results for ^{93}Tc

According to Nuclear Data Sheets [28] the available information about the yrast states of ^{93}Tc consists of a positive-parity cascade $\frac{25}{2}^+$ (4257 keV), $\frac{21}{2}^+$ (2535 keV), $\frac{17}{2}^+$ (2185 keV), $\frac{13}{2}^+$ (1434 keV) to the $\frac{9}{2}^+$ ground state and a negative-parity cascade $\frac{25}{2}^-$ (3889 keV), $\frac{21}{2}^-$ (3281 keV), $\frac{17}{2}^-$ (2185 keV), $\frac{13}{2}^-$ (2145 keV). The two $\frac{17}{2}$ states are very close. The $\frac{17}{2}^-$ state, only 0.44 keV above the $\frac{17}{2}^+$ state, is isomeric, half-life 10.2 μs, and decays to the $\frac{13}{2}^-$ and $\frac{13}{2}^+$ level [19]. The half-life of the $\frac{21}{2}^+$ level is 1.61 ns [29].

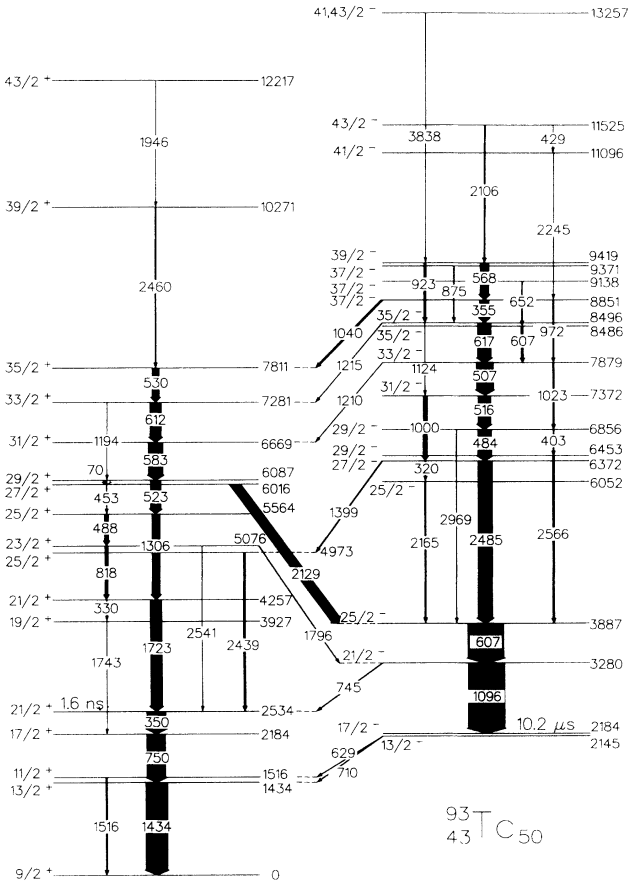

FIG. 2. Tentative level scheme of ^{93}Tc as populated in the $^{58}\mathrm{Ni}(^{40}\mathrm{Ca},5p)^{93}\mathrm{Tc}$ reaction. The widths of the arrows are roughly proportional to the γ-ray intensities; they are not corrected for the about 100-fold reduction caused by the 10.2-μs half-life of the 2184-keV level. Energies are in keV.

Table II gives the γ-ray energies, relative intensities, intensity anisotropies, and the placement of the transitions in the proposed level scheme of ^{93}Tc (see Fig. 2). Figure 3 shows a few $\gamma\gamma$-coincidence spectra. A plot of the R values is given in Fig. 4.

Concerning the 1723-keV γ ray, our R value 1.69±0.09 agrees well with the angular distribution coefficients obtained in the $(\alpha, p2n)$ reaction [18], viz. $a_2 = +0.40\pm0.04$, $a_4 = -0.06\pm0.08$. When plane polarization results are not available, the usual interpretation of such numbers is that the transition is a stretched $E2$. It can, however, as well be a $J \rightarrow J$ transition with dominating dipole part. There are strong theoretical grounds [12] to prefer this latter interpretation, implying a $\frac{21}{2}^+$ assignment to the 4257-keV level.

After the completion of our work on the decay scheme of ^{93}Tc, a paper by Ghugre *et al.* [20] about the high-spin states of this nucleus was published. Their results, although less detailed, are rather similar to ours, with, however, two important exceptions: high-energy γ-ray transitions ($E_\gamma > 2$ MeV) have escaped their observation, and the 1723-keV transition is interpreted (as in Ref. [18]) as a stretched $E2$ transition from a $\frac{25}{2}^+$ level.

TABLE II. Gamma-ray energies, intensities, and anisotropy ratios for γ-ray transitions assigned to ^{93}Tc.

E_γ[a] (keV)	I_γ[b]	R[c]	Tentative assignment $J_i^\pi \to J_f^\pi$	E_γ[a] (keV)	I_γ[b]	R[c]	Tentative assignment $J_i^\pi \to J_f^\pi$
70.4	87(4)	0.75(7)	$\frac{29}{2}^+ \to \frac{27}{2}^+$	972.1	95(5)	1.30(12)	$\frac{37}{2\ 1}^- \to \frac{33}{2}^-$
319.8	36(3)	0.81(11)	$\frac{27}{2}^- \to \frac{25}{2\ 2}^-$	1000.4	133(5)	1.70(13)	$\frac{31}{2}^- \to \frac{27}{2}^-$
329.6	22(2)	0.88(15)	$\frac{21}{2\ 2}^+ \to \frac{19}{2}^+$	1023.3	67(4)	1.05(11)	$\frac{33}{2}^- \to \frac{29}{2\ 2}^-$
349.9	474(8)	1.33(3)[e]	$\frac{21}{2\ 1}^+ \to \frac{17}{2}^+$	1040.3	79(4)	0.77(8)	$\frac{37}{2\ 1}^- \to \frac{35}{2}^+$
354.8	295(6)	0.78(2)	$\frac{37}{2\ 1}^- \to \frac{35}{2\ 2}^-$	1095.6	1000(11)	1.64(4)	$\frac{21}{2}^- \to \frac{17}{2}^-$
403.1	38(3)	2.12(32)	$\frac{29}{2\ 2}^- \to \frac{29}{2\ 1}^-$	1124.1	20(4)	1.64(57)	$\frac{35}{2\ 2}^- \to \frac{31}{2}^-$
428.6	9(3)	0.29(24)	$\frac{43}{2}^- \to \frac{41}{2}^-$	1194.2	9(4)		$\frac{33}{2}^+ \to \frac{29}{2}^+$
452.8	59(3)	1.26(11)	$\frac{27}{2}^+ \to \frac{25}{2\ 2}^+$	1209.5	18(6)		$\frac{33}{2}^- \to \frac{31}{2}^+$
483.8	403(9)	0.83(3)	$\frac{29}{2\ 2}^- \to \frac{27}{2}^-$	1215.2	15(6)		$\frac{35}{2\ 2}^- \to \frac{33}{2}^+$
487.9	124(4)	0.80(5)	$\frac{25}{2\ 2}^+ \to \frac{23}{2}^+$	1306.3	226(8)	1.53(8)	$\frac{25}{2\ 2}^+ \to \frac{21}{2\ 2}^+$
506.8	446(8)	0.72(2)	$\frac{33}{2}^- \to \frac{31}{2}^-$	1399.2	28(4)	0.85(19)	$\frac{27}{2}^- \to \frac{25}{2\ 1}^+$
516.5	360(7)	0.76(3)	$\frac{31}{2}^- \to \frac{29}{2\ 2}^-$	1434.3	540(11)	1.34(5)[e]	$\frac{13}{2}^+ \to \frac{9}{2}^+$
523.1	398(7)	1.58(5)	$\frac{29}{2}^+ \to \frac{25}{2\ 2}^+$	1516.2	5(3)		$\frac{11}{2}^+ \to \frac{9}{2}^+$
529.7	221(5)	0.68(3)	$\frac{35}{2}^+ \to \frac{33}{2}^+$	1723.0	365(9)	1.69(9)	$\frac{21}{2\ 2}^+ \to \frac{21}{2\ 1}^+$
568.2	278(6)	0.55(2)	$\frac{39}{2}^- \to \frac{37}{2\ 1}^-$	1743.1	19(4)	1.23(50)	$\frac{19}{2}^+ \to \frac{17}{2}^+$
582.7	418(8)	0.70(3)	$\frac{31}{2}^+ \to \frac{29}{2}^+$	1795.9	30(11)		$\frac{23}{2}^+ \to \frac{21}{2}^-$
607.3[d]			$\frac{35}{2\ 1}^- \to \frac{33}{2}^-$	1946.0	16(6)	1.65(17)[f]	$\frac{43}{2}^+ \to \frac{39}{2}^+$
	1011(15)	1.52(3)		2105.8	51(5)	1.45(15)[f]	$\frac{43}{2}^- \to \frac{39}{2}^-$
607.5[d]			$\frac{25}{2\ 1}^- \to \frac{21}{2}^-$	2129.5	208(8)	0.87(6)	$\frac{27}{2}^+ \to \frac{25}{2\ 1}^-$
611.5	343(7)	0.68(2)	$\frac{33}{2}^+ \to \frac{31}{2}^+$	2164.9	49(4)	1.80(33)	$\frac{25}{2\ 2}^- \to \frac{25}{2\ 1}^-$
617.2	397(7)	0.73(2)	$\frac{35}{2\ 2}^- \to \frac{33}{2}^-$	2245.5	12(6)		$\frac{41}{2}^- \to \frac{37}{2\ 1}^-$
628.5	10(4)		$\frac{13}{2}^- \to \frac{11}{2}^+$	2438.5	64(4)	1.44(19)	$\frac{25}{2\ 1}^+ \to \frac{21}{2\ 1}^+$
652.1	30(8)		$\frac{37}{2\ 2}^- \to \frac{35}{2\ 1}^-$	2460.2	53(4)	1.74(15)[f]	$\frac{39}{2}^+ \to \frac{35}{2}^+$
710.4	11(4)		$\frac{13}{2}^- \to \frac{13}{2}^+$	2484.8	472(11)	0.83(4)	$\frac{27}{2}^- \to \frac{25}{2\ 1}^-$
745.2	17(6)		$\frac{21}{2}^- \to \frac{21}{2\ 1}^+$	2541.3	12(7)		$\frac{23}{2}^+ \to \frac{21}{2\ 1}^+$
750.1	498(10)	1.27(4)[e]	$\frac{17}{2}^+ \to \frac{13}{2}^+$	2565.6	72(18)	1.54(25)	$\frac{29}{2\ 1}^- \to \frac{25}{2\ 1}^-$
818.2	125(5)	0.70(6)	$\frac{23}{2}^+ \to \frac{21}{2\ 2}^+$	2968.9	10(3)	1.63(53)	$\frac{29}{2\ 2}^- \to \frac{25}{2\ 1}^-$
874.9	24(3)	0.60(15)	$\frac{37}{2\ 3}^- \to \frac{35}{2\ 2}^-$	3837.6	6(4)	1.19(3)[f]	$\frac{(41,43)}{2}^- \to \frac{39}{2}^-$
923.2	72(4)	1.37(15)	$\frac{39}{2}^- \to \frac{35}{2\ 2}^-$				

[a] $\Delta E_\gamma = \pm(0.2\text{–}1.0)$ keV depending on the energy and intensity of the transition.
[b] The γ-ray intensity, I_γ, is corrected for detection efficiency and is normalized to 1000 for the 1095.6-keV transition.
[c] The γ-ray anisotropy is defined as $R = 2I(143°)/[I(79°) + I(101°)]$.
[d] Not resolved.
[e] R value low (1.31±0.03) due to the half-life of the 2534-keV level.
[f] R value from stacked target run.

These two differences have important consequences for the interpretation of the results, as it leads to their missing of energy gaps, also at relatively low excitation energy, making part of the discussion inadequate. Also the comparison with shell-model calculations will be affected by their interpretation of the multipolarity of the 1723-keV transition.

A minor (31 keV) discrepancy in the energies of the $\frac{21}{2}^-$ and $\frac{25}{2}^-$ levels is due to their neglect of the work of Brown *et al.* [19]. In our measurements the order between the 818- and 488-keV transitions could be chosen on the basis of the weak 1796-keV $E1$ branch; this also fixed the order between the 1306- and 523-keV lines. In the negative-parity cascade, the only minor differences are the positions of the weak part of the 607-keV doublet and the weak 320-keV line. Ghugre *et al.* [20] did observe the 403-keV line but could not find a place for it, nor could they explain the coincidences in the gates set on the 582-,

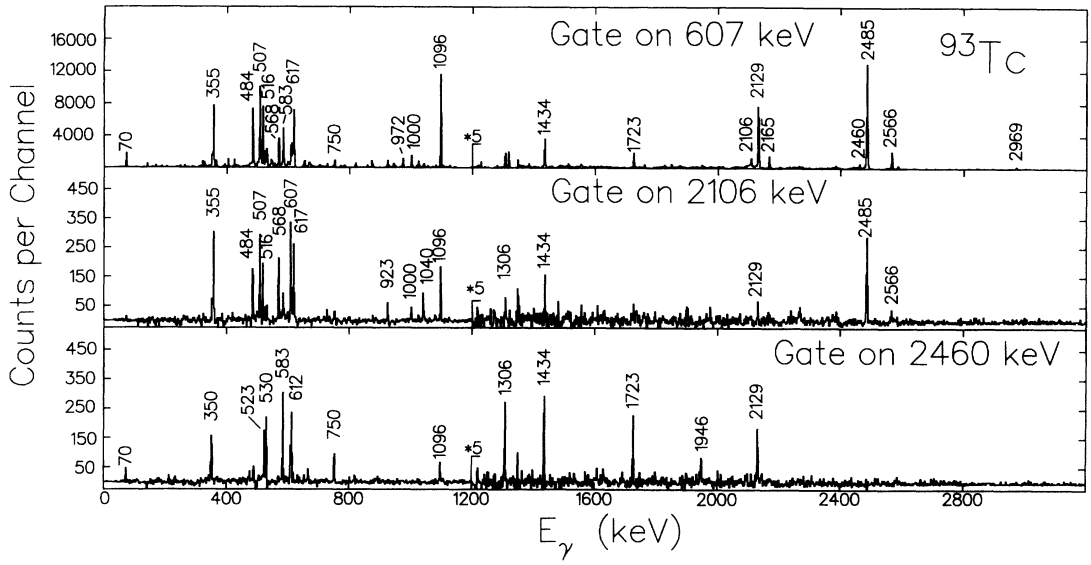

FIG. 3. Typical $\gamma\gamma$-coincidence spectra of ^{93}Tc from thick target run.

611-, and 529-keV γ rays.

It could be remarked in this connection that already in the ^{92}Mo$(\alpha, p2n)^{93}$Tc reaction several γ rays did show up clearly in the spectra ([18], Fig. 1, and Table III), but could not be placed with the two-detector coincidence technique available at that time. This is evident up to and including the $\frac{31}{2}^+$ and $\frac{29}{2}^-$ levels. Thus, the increase of angular momentum input from about 15–20 units to about 56 units has yielded less than 50% increase in the observed level spin, a rather noteworthy fact.

It is also notable that the $\frac{39}{2}^+$ level is much less populated than the $\frac{39}{2}^-$ one; in the five other cascades observed in the present work the big jump in the γ-ray flow occurs at the spin and parity given in the last column of Table I.

The half-life of the first $\frac{21}{2}^+$ level was found to be 1.82±0.1 ns, in agreement with the value 1.61±0.10 ns obtained in Ref. [29] by direct timing (the value, uncorrected for deorientation, was 1.77 ns).

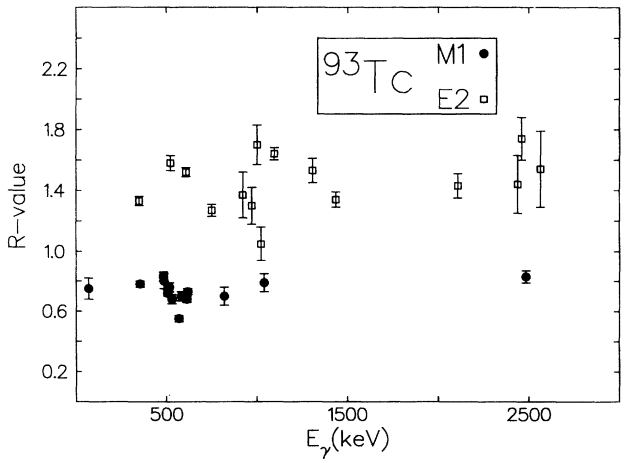

FIG. 4. Gamma-ray anisotropies, R (see text), plotted against the energy of the γ-ray transitions in ^{93}Tc. Only γ rays for which $I_\gamma > 0.05\ I(1096\ \text{keV})$ are included.

B. Results for ^{94}Ru

The level scheme of ^{94}Ru deduced from the present work is displayed in Fig. 5. Figure 6 shows some coincidence spectra and Table III gives the γ-ray energies, relative intensities, anisotropies, and the placement of the transitions in the proposed level scheme. A plot of the R values is given in Fig. 7.

The agreement with the level scheme proposed by Nolte *et al.* [15] is complete for the positive-parity cascade downwards from the 9041-keV level (17^+) and from the 5568-keV level (13^-) for the negative-parity cascade.

A number of isomeric states are established in ^{94}Ru [15]. In the positive-parity cascade the following half-lives are known: the 6^+ state at 2498 keV, 70 ns, the 8^+ state at 2645 keV, 71 μs, and the 12^+ state at 4717 keV, 35 ps. In the negative-parity cascade the 5^- state at 2625 keV has a half-life of about 0.5 ns and the 11^- state at 4489 keV a half-life of 780 ps.

In a comparison with the level scheme proposed by Piel *et al.* [16], we agree about the positions of the 19^+ and 18^+ states (9920 and 9526 keV, respectively). The 13^- state is also proposed there at 5568 keV.

The observation of the weak crossover transitions in the present work firmly establishes the order of the dipole transitions and hence the levels in the positive-parity cascade between spins 13^+ and 20^+.

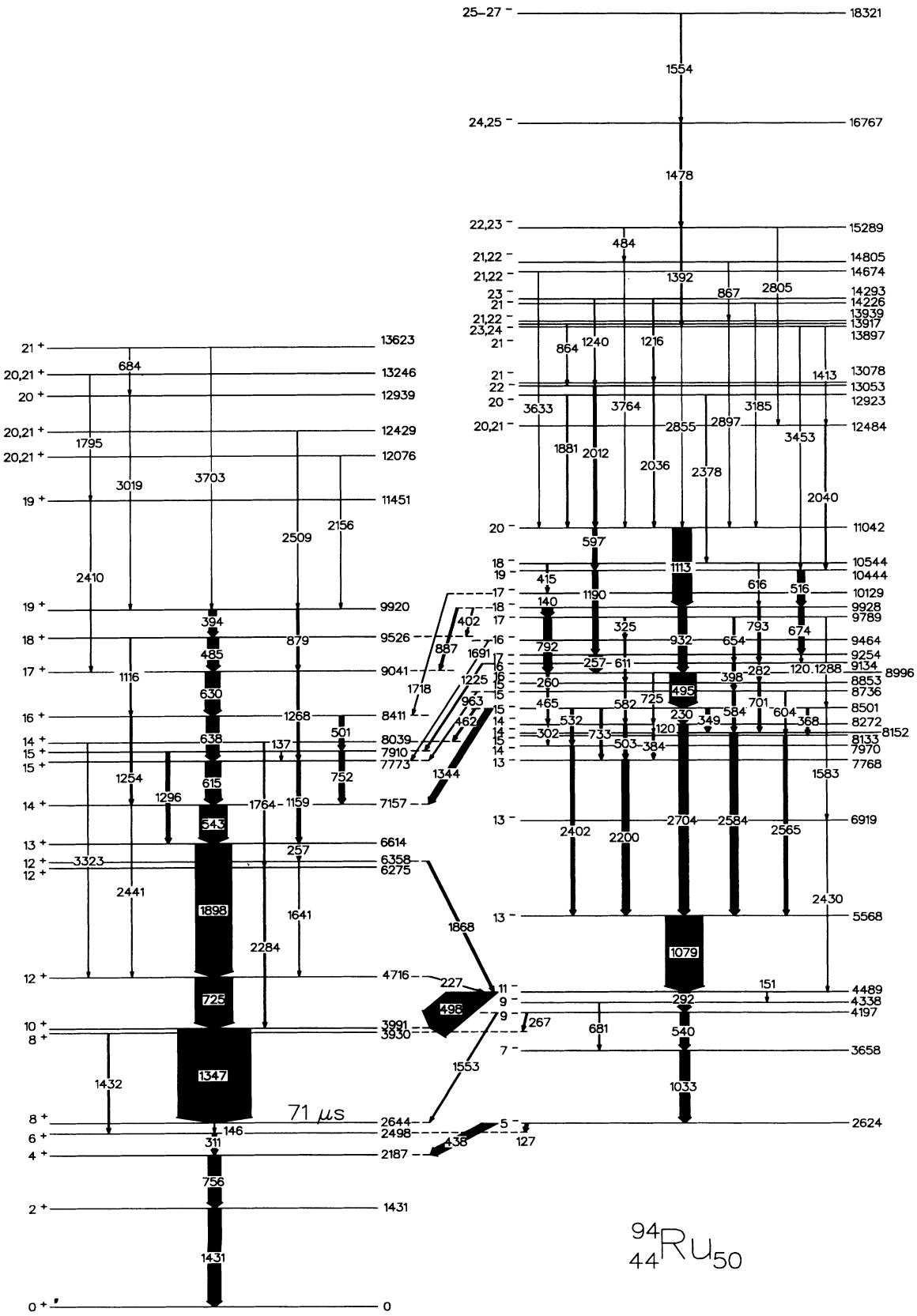

FIG. 5. Tentative level scheme of ^{94}Ru as produced in the ^{58}Ni(^{40}Ca,4p)^{94}Ru reaction. Energies in keV. The widths of the arrows are roughly proportional to the γ-ray intensities; they are not corrected for the about 700-fold reduction caused by the 71-μs half-life [15] of the 2644-keV level.

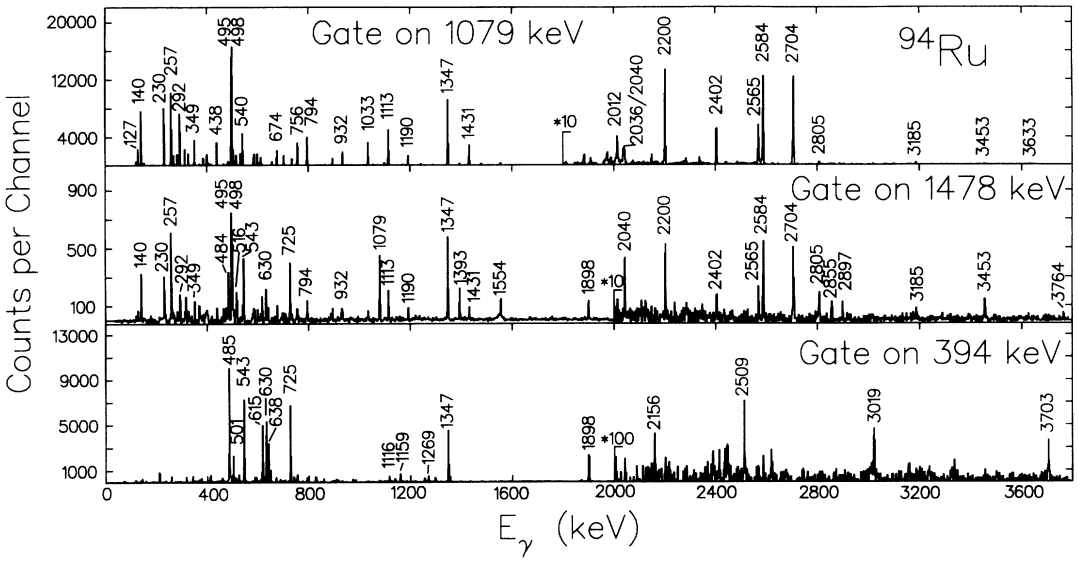

FIG. 6. Typical $\gamma\gamma$-coincidence spectra of ^{94}Ru.

TABLE III. Gamma-ray energies, intensities, and anisotropy ratios for γ-ray transitions assigned to ^{94}Ru.

E_γ[a] (keV)	I_γ[b]	R[c]	Tentative assignment $J_i^\pi \to J_f^\pi$	E_γ[a] (keV)	I_γ[b]	R[c]	Tentative assignment $J_i^\pi \to J_f^\pi$
119.7[d]	11(1)	0.76(11)	$17_1^- \to 16_2^-$	501.0[d]	71(2)	0.72(4)	$16^+ \to 15_2^+$
120.1[d]	13(1)		$14_3^- \to 14_2^-$	503.3[d]			$14_3^- \to 13_3^-$
126.5	52(2)	0.81(6)	$5^- \to 6^+$	510.8	31(2)	1.05(11)	
137.0	7(1)		$15_2^+ \to 15_1^+$	515.6	103(3)	0.81(5)	$19^- \to 18_1^-$
139.6	168(2)	0.82(2)	$18_1^- \to 17_2^-$	531.6	47(2)	0.90(7)	$15_2^- \to 14_1^-$
146.1	2(1)		$8_1^+ \to 6^+$	539.6	179(3)	1.25(3)	$9_1^- \to 7^-$
150.7	7(1)	1.18(26)	$11^- \to 9_2^-$	543.0	362(4)	0.81(2)	$14_1^+ \to 13^+$
227.4	8(1)		$12_1^+ \to 11^-$	581.8	27(3)	0.77(16)	$15_4^- \to 14_3^-$
229.8	153(3)	0.87(3)	$15_2^- \to 14_3^-$	584.2	58(3)	0.79(7)	$15_3^- \to 14_2^-$
256.7[d]			$13^+ \to 12_3^+$	597.5	74(3)	1.42(8)	$20_1^- \to 19^-$
257.3[d]	245(2)	0.82(2)	$17_1^- \to 16_1^-$	603.7	13(3)		$15_3^- \to 15_1^-$
259.7	41(2)	0.89(5)	$16_1^- \to 15_3^-$	610.6	49(3)	0.57(7)	$16_3^- \to 15_4^-$
267.2	24(1)	1.08(8)	$9_1^- \to 8_2^+$	615.3[d]	223(4)	0.67(2)	$15_1^+ \to 14_1^+$
281.6	30(1)	0.78(5)	$16_2^- \to 15_4^-$	615.7[d]			$18_2^- \to 18_1^-$
291.7	198(2)	1.34(3)	$11^- \to 9_1^-$	630.2	212(3)	0.72(2)	$17^+ \to 16^+$
301.7	8(2)		$14_3^- \to 14_1^-$	638.0	165(3)	0.72(2)	$16^+ \to 15_1^+$
311.4	66(2)	1.25(6)	$6^+ \to 4^+$	654.1	36(2)	0.68(6)	$17_2^- \to 16_2^-$
325.2	33(2)	0.90(6)	$17_2^- \to 16_3^-$	674.4	104(3)	1.76(5)	$18_1^- \to 17_1^-$
349.0	60(3)	0.60(5)	$15_2^- \to 14_2^-$	680.9	16(2)	1.14(19)	$9_2^- \to 7^-$
368.3	43(2)	1.60(9)	$15_2^- \to 15_1^-$	683.8			$21^+ \to 20^+$
383.9	27(3)		$14_2^- \to 13_3^-$	701.1	39(3)	0.94(10)	$15_4^- \to 14_2^-$
394.3	92(3)	0.76(4)	$19_1^+ \to 18^+$	707.7	18(2)	0.59(10)	
398.1	41(2)	0.85(6)	$16_2^- \to 15_3^-$	725.0[d]			$16_1^- \to 14_3^-$
401.9	17(2)	0.86(13)	$18_1^- \to 18^+$	725.3[d]	518(5)	1.62(3)	$12_1^+ \to 10^+$
415.4	25(2)	0.77(9)	$18_2^- \to 17_3^-$	733.3	43(2)	1.56(11)	$15_2^- \to 13_3^-$
437.7	113(3)	1.09(4)	$5^- \to 4^+$	752.1	82(2)	0.73(4)	$15_2^+ \to 14_1^+$
461.9	37(3)	0.68(8)	$15_2^- \to 14_2^+$	755.9	198(3)	1.24(3)	$4^+ \to 2^+$
464.8	31(2)	0.68(9)	$15_3^- \to 14_3^-$	792.4[d]	179(3)	0.81(3)	$17_2^- \to 16_1^-$
483.8[d]			$(22,23)^- \to (21,22)_3^-$	793.4[d]			$18_1^- \to 16_2^-$
484.7[d]	143(4)	0.76(3)	$18^+ \to 17^+$	863.6	17(3)	0.86(24)	$(23,24)^- \to 22^-$
495.0	396(5)	0.76(2)	$16_1^- \to 15_2^-$	867.0	11(3)	1.37(48)	$(21,22)_3^- \to (21,22)_1^-$
498.0	423(4)	0.98(2)	$11^- \to 10^+$	879.3	29(3)	2.07(29)	$19_1^+ \to 17^+$

TABLE III. *(Continued).*

E_γ[a] (keV)	I_γ[b]	R[c]	Tentative assignment $J_i^\pi \to J_f^\pi$	E_γ[a] (keV)	I_γ[b]	R[c]	Tentative assignment $J_i^\pi \to J_f^\pi$
886.8	31(3)	0.87(10)	$18_1^- \to 17^+$	1795.3	6(2)		$(20,21)_3^+ \to 19_2^+$
931.9	135(3)	1.48(6)	$18_1^- \to 16_1^-$	1868.5	33(3)	0.76(10)	$12_3^+ \to 11^-$
963.4	13(3)	0.82(33)	$15_3^- \to 15_1^+$	1881.3	22(2)	1.18(19)	$20_2^- \to 20_1^-$
1033.3	186(3)	1.28(4)	$7^- \to 5^-$	1897.9	483(6)	1.00(2)	$13^+ \to 12_1^+$
1078.8	590(5)	1.61(3)	$13_1^- \to 11^-$	1907.1	11(2)	0.79(25)	
1113.4[d]	338(5)	1.54(4)	$20_1^- \to 18_1^-$	2011.6	52(3)	1.40(13)	$22^- \to 20_1^-$
1115.6[d]			$18^+ \to 16^+$	2035.8	19(2)	0.73(14)	$21_1^- \to 20_1^-$
1158.8	53(3)	1.59(14)	$15_1^+ \to 13^+$	2039.9	28(2)	1.16(36)	$(20,21)^- \to 19^-$
1168.8	15(2)	1.22(20)		2156.2	6(3)		$(20,21)_1^+ \to 19_1^+$
1190.4	98(3)	1.49(7)	$19^- \to 17_1^-$	2200.4	130(3)	1.67(8)	$13_3^- \to 13_1^-$
1215.8	17(3)		$23^- \to 21_1^-$	2283.8	31(3)	1.03(14)	$12_2^+ \to 10^+$
1225.1	11(2)	0.82(21)	$16_2^- \to 15_2^+$	2377.6	19(2)	1.19(21)	$20_2^- \to 18_2^-$
1240.1	12(2)	0.73(18)	$23^- \to 22^-$	2402.0	55(3)	0.40(4)	$14_1^- \to 13_1^-$
1253.8	28(2)	1.88(23)	$16^+ \to 14_1^+$	2410.0	10(2)	1.27(36)	$19_2^+ \to 17^+$
1268.5	25(2)	1.92(27)	$17^+ \to 15_1^+$	2430.0	10(2)		$13_2^- \to 11^-$
1288.0	15(2)	0.68(11)	$17_2^- \to 15_2^-$	2440.8	10(2)		$14_1^+ \to 12_1^+$
1295.5	51(3)	1.30(13)	$15_2^+ \to 13^+$	2508.6	9(3)		$(20,21)_2^+ \to 19_1^+$
1344.0	102(3)	1.01(5)	$15_2^- \to 14_1^+$	2565.4	65(3)	1.71(12)	$15_1^- \to 13_1^-$
1347.1	1000(6)	1.46(2)	$10^+ \to 8_1^+$	2584.5	123(3)	0.86(4)	$14_2^- \to 13_1^-$
1392.6	31(4)	1.06(21)	$(22,23)^- \to 21_2^-$	2704.1	153(3)	0.93(4)	$14_3^- \to 13_1^-$
1412.9	9(4)		$21_2^- \to (20,21)^-$	2805.2	7(2)		$(22,23)^- \to (20,21)^-$
1430.7	241(5)	1.20(5)	$2^+ \to 0^+$	2854.7	6(2)		$21_2^- \to 20_1^-$
1432.1	6(3)		$8_2^+ \to 6^+$	2897.1	7(2)		$(21,22)_1^- \to 20_1^-$
1477.9	40(2)	1.29(9)	$(24,25)^- \to (22,23)^-$	3019.0	7(2)	0.58(24)	$20^+ \to 19_1^+$
1553.2[d]	30(2)	1.07(10)	$9_1^- \to 8_1^+$	3184.8	5(2)	0.60(21)	$21_3^- \to 20_1^-$
1554.0[d]			$(25-27)^- \to (24,25)^-$	3322.7	6(1)	1.85(48)	$14_2^+ \to 12_1^+$
1582.8	9(3)		$15_2^- \to 13_2^-$	3452.6	7(2)	1.24(57)	$21_2^- \to 19^-$
1641.0	11(2)	1.37(38)	$12_3^+ \to 12_1^+$	3632.9	4(1)	0.71(30)	$(21,22)_2^- \to 20_1^-$
1691.0	4(2)		$16_3^- \to 15_1^+$	3702.8	4(1)	1.46(52)	$21^+ \to 19_1^+$
1718.3	6(3)		$17_3^- \to 16^+$	3763.7	3(1)		$(21,22)_3^- \to 20_1^-$
1764.3	12(2)	1.80(56)	$14_2^+ \to 12_2^+$				

[a] $\Delta E_\gamma = \pm(0.2\text{–}1.0)$ keV depending on the energy and intensity of the transition.
[b] The γ-ray intensity, I_γ, is corrected for detection efficiency and is normalized to 1000 for the 1347.1-keV transition.
[c] The γ-ray anisotropy is defined as $R = 2I(143°)/[I(79°) + I(101°)]$.
[d] Not resolved.

Further, summed intensities of the high-energy transitions in the range 2–3 MeV directly feeding the 13^- state and not observed in previous works [15,16] indicate that the low-energy transitions observed in coincidence with the 1079-keV line which deexcites the 13^- state should be placed much higher up in the negative-parity cascade.

Since Piel *et al.* [16] did not find a place for the 501-keV γ ray, they made the wrong choice for the position of the 16^+ level, and they did not observe the decay of the weakly populated 8_2^+, 12_2^+, 12_3^+, and 14_2^+ levels at all.

Concerning the negative-parity states, we agree with Refs. [15,16] up to and including the 13^- level at 5568 keV, except that we find a second 9^- level at 4338 keV. The $B(E2)$ values for the two transitions from the 11^- level are equal within errors (cf. the discussion). Above 5568 keV, a number of transitions of 2–3 MeV depopulate a large number of close-lying levels, which have not been reported before. A few of the transitions between these levels were seen also in Ref. [16], but placed in other ways.

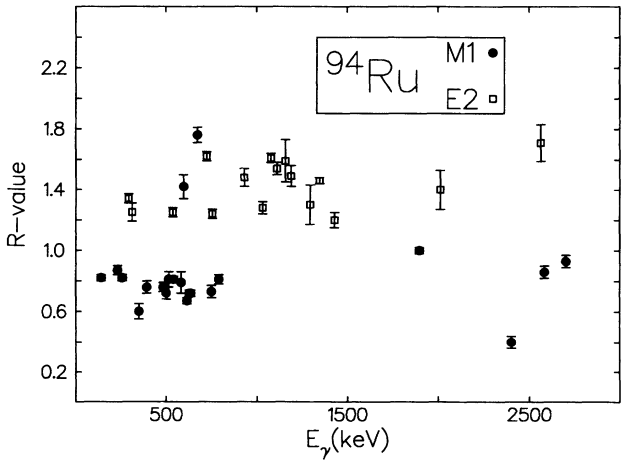

FIG. 7. Gamma-ray anisotropies, R (see text), plotted against the energies of the γ-ray transitions in ^{94}Ru. Only γ rays for which $I_\gamma > 0.05\ I(1347\text{ keV})$ are included.

C. Results for ^{95}Rh

From the coincidence measurements and the γ-ray anisotropies we obtain the level scheme of ^{95}Rh displayed in Fig. 8. Two coincidence spectra are presented in Fig. 9 and a plot of the R values in Fig. 10. The information obtained is presented in Table IV.

Two isomeric states were found by Nolte *et al.* [15]. The $\frac{17}{2}^-$ state at 2236 keV has a half-life of 19 ns [30] and the $\frac{21}{2}^+$ state at 2448 keV a half-life of 2.1 ns. The agreement with the level scheme proposed by Nolte *et al.* [15] is almost complete up to spin values of $\frac{25}{2}^+$ and $\frac{25}{2}^-$, the only exception being that we find a second $\frac{17}{2}^+$ level at 2463 keV. The $B(E2)$ value of the 185-keV transition from the $\frac{21}{2}^+$ level at 2448 keV is about four times larger than that of the 381-keV transition (see the discussion), viz. 4.5 W.u. against 1.05 W.u.

Not having noted the 2489-keV line, Nolte *et al.* [15] placed the higher γ rays in the wrong order and were, e.g., not able to find the $\frac{25}{2}^+_2$ level at 5457 keV. For this and higher levels in the positive-parity cascade, our ordering of γ rays is supported by a number of weak transitions.

As could be expected, also the negative-parity structure of ^{95}Rh is quite similar to that of ^{93}Tc, with the $\frac{25}{2}^- \rightarrow \frac{21}{2}^- \rightarrow \frac{17}{2}^-$ cascade at the bottom. The three weak transitions observed in Ref. [15] are now placed on top of the 7845-keV level; the other γ rays have not been reported before.

Just as for ^{93}Tc and ^{94}Ru there are intensity jumps high up in the level scheme. Thus, the visible $\frac{39}{2}^+$ level feeding is only one-third of what goes out, and the corresponding ratio for the $\frac{39}{2}^-$ level is little more than one-half.

TABLE IV. Gamma-ray energies, intensities, and anisotropy ratios for γ-ray transitions assigned to ^{95}Rh.

E_γ[a] (keV)	I_γ[b]	R[c]	Tentative assignment $J_i^\pi \rightarrow J_f^\pi$	E_γ[a] (keV)	I_γ[b]	R[c]	Tentative assignment $J_i^\pi \rightarrow J_f^\pi$
92.8	26(5)	0.56(20)	$\frac{29}{2}^+ \rightarrow \frac{27}{2}^+$	951.7	36(13)		$\frac{39}{2}^- \rightarrow \frac{35}{2}^-$
114.1	12(4)		$\frac{29}{2}^-_1 \rightarrow \frac{27}{2}^-$	1004.8	500(12)	1.66(8)	$\frac{21}{2}^- \rightarrow \frac{17}{2}^-$
169.0	372(11)	1.15(5)[d]	$\frac{17}{2}^- \rightarrow \frac{17}{2}^+_1$	1147.2	195(9)	1.54(14)	$\frac{33}{2}^- \rightarrow \frac{29}{2}^-_1$
185.2	47(6)	1.23(39)	$\frac{21}{2}^+_1 \rightarrow \frac{17}{2}^+_2$	1216.4	36(10)		$\frac{25}{2}^+_2 \rightarrow \frac{21}{2}^+_2$
261.0	252(10)	0.89(6)	$\frac{37}{2}^- \rightarrow \frac{35}{2}^-$	1250.1	183(13)	1.53(16)	$\frac{39}{2}^+ \rightarrow \frac{35}{2}^+$
293.8	47(9)		$\frac{29}{2}^-_1 \rightarrow \frac{25}{2}^-_2$	1274.7	429(16)	1.80(12)	$\frac{25}{2}^+_1 \rightarrow \frac{21}{2}^+_1$
333.3	78(9)	0.66(16)	$\frac{33}{2}^- \rightarrow \frac{31}{2}^-$	1306.7	35(11)		$\frac{41}{2}^- \rightarrow \frac{39}{2}^-$
344.4	96(11)	0.85(25)	$\frac{33}{2}^+ \rightarrow \frac{31}{2}^+$	1350.7	1000(17)	1.20(4)[d]	$\frac{13}{2}^+ \rightarrow \frac{9}{2}^+$
381.5	407(13)	1.36(7)	$\frac{21}{2}^+_1 \rightarrow \frac{17}{2}^+_1$	1441.8	29(10)		$\frac{(45,47)}{2}^+ \rightarrow \frac{43}{2}^+$
447.5	35(15)		$\frac{31}{2}^- \rightarrow \frac{29}{2}^-_2$	1734.4	254(12)	1.58(14)	$\frac{25}{2}^+_2 \rightarrow \frac{25}{2}^+_1$
467.6	37(12)		$\frac{43}{2}^+ \rightarrow \frac{41}{2}^+_1$	1792.7	33(10)	1.45(73)	$\frac{21}{2}^+_2 \rightarrow \frac{21}{2}^+_1$
479.4	50(11)	0.69(40)	$\frac{29}{2}^-_2 \rightarrow \frac{27}{2}^-$	1997.3	15(9)		$\frac{41}{2}^- \rightarrow \frac{37}{2}^-$
485.6	112(18)	0.63(20)	$\frac{35}{2}^+ \rightarrow \frac{33}{2}^+$	2021.4	49(13)		$\frac{(41,43)}{2}^-_1 \rightarrow \frac{39}{2}^-$
548.9	259(18)	1.12(16)	$\frac{35}{2}^- \rightarrow \frac{33}{2}^-$	2396.1	22(7)		$\frac{27}{2}^+ \rightarrow \frac{25}{2}^+_1$
582.9	362(20)	0.69(7)	$\frac{31}{2}^+ \rightarrow \frac{29}{2}^+$	2488.5	142(12)	1.72(29)	$\frac{29}{2}^+ \rightarrow \frac{25}{2}^+_1$
661.3	57(10)	0.68(22)	$\frac{27}{2}^+ \rightarrow \frac{25}{2}^+_2$	2496.4	73(8)	1.94(44)	$\frac{25}{2}^-_2 \rightarrow \frac{25}{2}^-_1$
667.4	504(18)	1.48(9)	$\frac{25}{2}^-_1 \rightarrow \frac{21}{2}^-$	2676.6	37(6)		$\frac{27}{2}^- \rightarrow \frac{25}{2}^-_1$
690.5	193(12)	0.87(10)	$\frac{39}{2}^- \rightarrow \frac{37}{2}^-$	2790.3	206(9)	1.73(9)	$\frac{29}{2}^-_1 \rightarrow \frac{25}{2}^-_1$
716.2	901(21)	1.14(4)[d]	$\frac{17}{2}^+_1 \rightarrow \frac{13}{2}^+$	2848.1	16(8)		$\frac{(41,43)}{2}^-_2 \rightarrow \frac{39}{2}^-$
753.7	196(15)	2.10(31)	$\frac{29}{2}^+ \rightarrow \frac{25}{2}^+_2$	3091.9	24(7)		$\frac{41}{2}^+_1 \rightarrow \frac{39}{2}^+$
769.9	26(10)		$\frac{35}{2}^- \rightarrow \frac{35}{2}^+$	3238.6	19(8)	0.56(30)	$\frac{41}{2}^+_2 \rightarrow \frac{39}{2}^+$
809.7	30(11)	1.60(94)	$\frac{37}{2}^- \rightarrow \frac{33}{2}^-$	3522.4	10(4)		$\frac{(41,43)}{2}^-_3 \rightarrow \frac{39}{2}^-$
813.3	29(10)		$\frac{31}{2}^- \rightarrow \frac{29}{2}^-_1$	3559.2	17(4)	1.37(66)	$\frac{43}{2}^+ \rightarrow \frac{39}{2}^+$
830.1	253(12)	1.71(15)	$\frac{35}{2}^+ \rightarrow \frac{31}{2}^+$				
912.9	76(16)	1.99(88)	$\frac{17}{2}^+_2 \rightarrow \frac{13}{2}^+$				

[a] $\Delta E_\gamma = \pm(0.2\text{–}1.0)$ keV depending on the energy and intensity of the transition.
[b] The γ-ray intensity, I_γ, is corrected for detection efficiency and is normalized to 1000 for the 1350.7-keV transition.
[c] The γ-ray anisotropy is defined as $R = 2I(143°)/[I(79°) + I(101°)]$.
[d] R value low due to the half-life of the 2236-keV level.

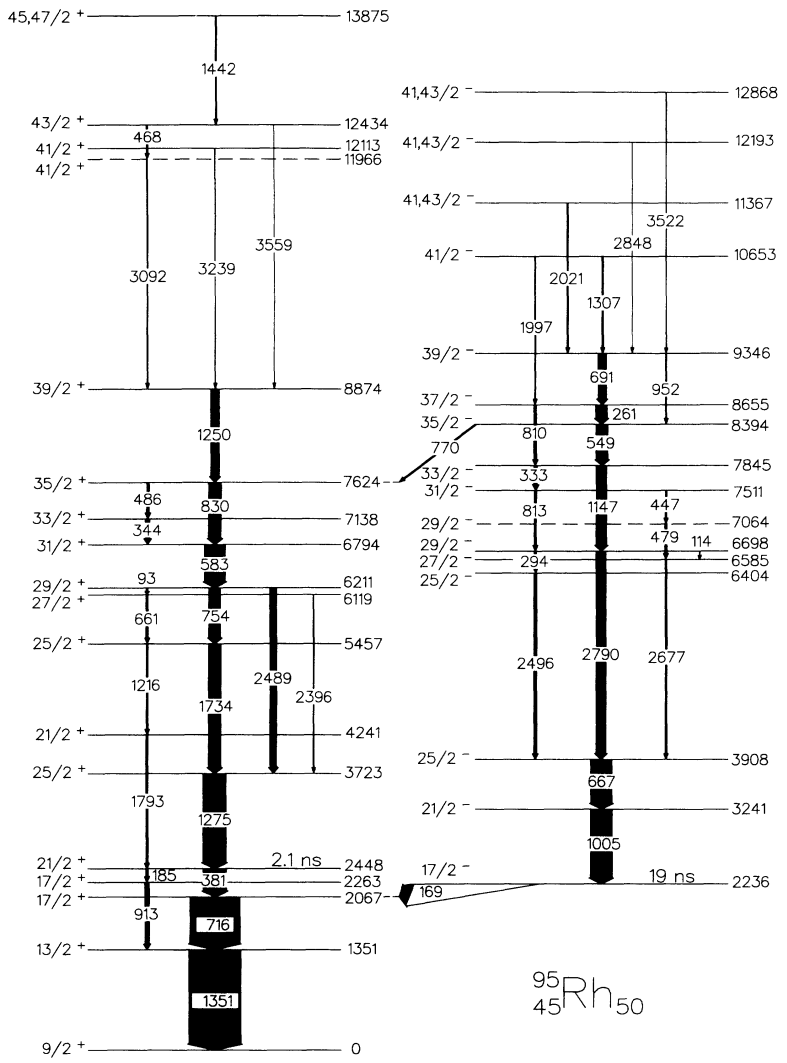

FIG. 8. Tentative level scheme for ^{95}Rh as produced in the ^{58}Ni(^{40}Ca,3p)^{95}Rh reaction. The widths of the arrows are roughly proportional to the γ-ray intensities. Energies are in keV.

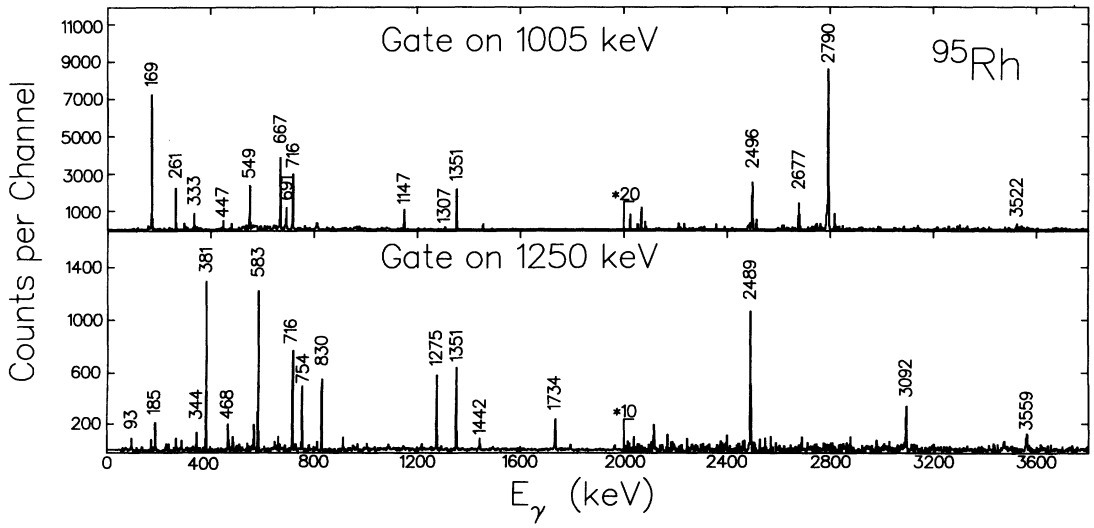

FIG. 9. Typical $\gamma\gamma$-coincidence spectra of ^{95}Rh.

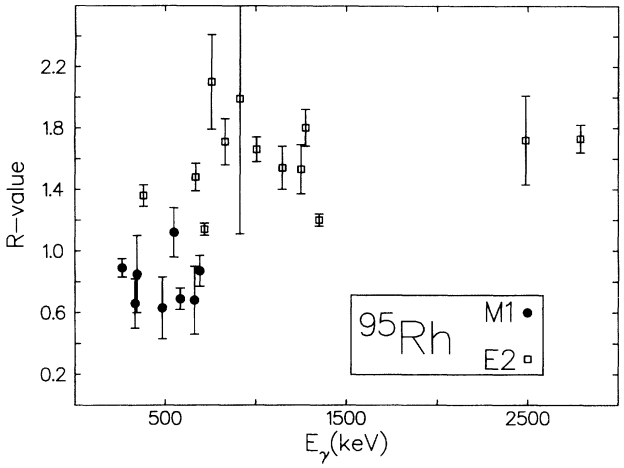

FIG. 10. Gamma-ray anisotropies, R (see text), plotted against the energies of the γ-ray transitions in ^{95}Rh. Only γ rays for which $I_\gamma > 0.05\ I(1351\ \text{keV})$ are included.

IV. DISCUSSION

The use of multidetector arrays allows the yrast level schemes to be determined up to and in favorable cases above the spin values corresponding to the highest angular momenta attainable with the configuration spaces used in shell-model calculations. Thus, we can now compare experimental and theoretical yrast levels over a large range of excitation energy.

The maximum angular momenta that can be generated in model spaces limited to the orbitals $p_{1/2}$, $g_{9/2}$, or $f_{5/2}$, $p_{3/2}$, $p_{1/2}$, $g_{9/2}$, or $p_{1/2}$, $g_{9/2}$, $d_{5/2}$ are given in Table I. The experimental maximum spin values can be compared with those given in the table, and it can be decided if the configuration space chosen is sufficient for description of the observed states.

As mentioned in the Introduction a large number of shell-model calculations have been performed for the N=50 nuclei [1–14]. All of these except one [11] have assumed a closed N=50 neutron core, and described the states at low excitation energy in terms of valence protons within the $p_{1/2}$, $g_{9/2}$ or $f_{5/2}$, $p_{3/2}$, $p_{1/2}$, $g_{9/2}$ shell groups. Comparisons of calculated and experimental energies show in general very good agreement, in particular for those calculations [8,12,13] which determine the effective two-body interaction matrix elements by fits to experimental energies. The present experiment has identified a large number of states in ^{93}Tc, ^{94}Ru, and ^{95}Rh at higher energy and spin, most of which can be described as a neutron particle-hole excitation $\nu d_{5/2} g_{9/2}^{-1}$ coupled to the valence proton states.

A. Discussion of levels of ^{93}Tc

The experimental level scheme in Fig. 2 is reproduced in a slightly truncated form in Fig. 11, with the levels ordered according to their structural character. The experimental excitation energies of the pure proton states are compared in Fig. 12 with the calculated energies from the recent work of Sinatkas *et al.* [14]. The agreement is very good, in particular for the yrast $\frac{9}{2}^+$, $\frac{13}{2}^+$, $\frac{17}{2}^+$, and $\frac{21}{2}^+$ states, which are dominated by the $p_{1/2}^2 g_{9/2}^3$ configuration. The agreement is less perfect for the $\frac{13}{2}^-$, $\frac{17}{2}^-$, $\frac{21}{2}^-$, $\frac{25}{2}^-$ states and the $\frac{25}{2}^+$ state, which belong to the $p_{1/2} g_{9/2}^4$ and $g_{9/2}^5$ configurations, respectively. This difference can be traced to the large spacing between the single-hole energies of $p_{1/2}^{-1}$ and $g_{9/2}^{-1}$ in ^{99}In, which was taken to be 1.85 MeV in [14], while the corresponding values are 0.39 MeV in [8], 0.33 MeV in [12], and 0.55 MeV in [13].

The highest-spin state of the $f_{5/2}^{-1} p_{1/2}^2 g_{9/2}^4$ configuration, which has been tentatively identified with the $\frac{29}{2}^-$ level at 6453 keV in Fig. 11, is calculated about 1 MeV too high [14]. Previously, there has been no experimental constraint of the $f_{5/2}^{-1}$ proton-hole energy in heavy N=50 isotones.

In order to interpret other states with spins $\leq \frac{39}{2}$, the proton configurations $\pi(p_{1/2}, g_{9/2})^5$ are combined with a neutron $\nu d_{5/2} g_{9/2}^{-1}$ excitation. The energies of such states have been calculated by Muto *et al.* [11]. This neutron configuration is the most relevant one for yrast and near-yrast states in ^{93}Tc, since $g_{9/2}^{-1}$ is the only high-spin hole orbital, and since $d_{5/2}$ is the lowest particle orbital above N=50, well separated in energy from the $g_{7/2}$ and $h_{11/2}$ orbitals. We associate the observed levels from $\frac{19}{2}^+$ to $\frac{35}{2}^+$ with the $\pi(p_{1/2}^2 g_{9/2}^3)\nu(d_{5/2} g_{9/2}^{-1})$ configuration, the levels from $\frac{25}{2}^-$ to $\frac{39}{2}^-$ with the $\pi(p_{1/2} g_{9/2}^4)\nu(d_{5/2} g_{9/2}^{-1})$ configuration, and the $\frac{39}{2}^+$ level at 10271 keV with the highest-spin member of the $\pi(g_{9/2}^5)\nu(d_{5/2} g_{9/2}^{-1})$ configuration. These assignments are indicated in Fig. 11.

The energies of the unique $\frac{35}{2}^+$, $\frac{39}{2}^-$, and $\frac{39}{2}^+$ states, which are the maximum-spin members of these three configurations, have been calculated by using the experimental energy of the $\nu(d_{5/2} g_{9/2}^{-1})7^+$ state in ^{88}Sr, adding the proton-neutron interaction energies derived from levels in N=49 and 51 nuclei. The calculated energies are 7850 keV ($\frac{35}{2}^+$), 9410 keV ($\frac{39}{2}^-$), and 10 060 keV ($\frac{39}{2}^+$). The good agreement with the experimental energies for the first two states gives a strong indication that these configuration assignments are correct. The agreement is less perfect for the $\frac{39}{2}^+$ state, leaving some uncertainty regarding the interpretation of this state.

The levels in the even-parity cascade below $\frac{35}{2}^+$ are suggested to belong to the $\pi(p_{1/2}^2 g_{9/2}^3)\nu(d_{5/2} g_{9/2}^{-1})$ configuration, from the strongly favored transitions between states within this group. $M1$ and $E2$ transitions to other states from the levels at 6087 keV ($\frac{29}{2}^+$), 6016 keV ($\frac{27}{2}^+$), 5564 keV ($\frac{25}{2}^+$), 5076 keV ($\frac{23}{2}^+$), and 4257 keV ($\frac{21}{2}^+$) are either not observed or proceed with very small relative transition rates. By similar arguments the levels in the odd-parity cascade at 9419, 8851, 8496, 7879, 7372, 6856, 6372, and 6052 keV are assigned to the

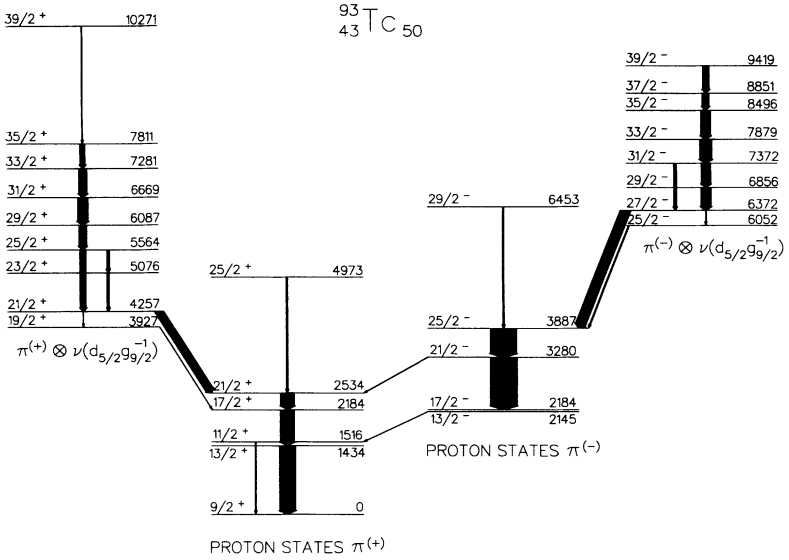

FIG. 11. Structural scheme for ^{93}Tc, showing a representative selection of levels and transitions.

$\pi(p_{1/2}g_{9/2}^4)\nu(d_{5/2}g_{9/2}^{-1})$ configuration. No firm interpretation is given for the weakly populated levels at 9371, 9138, and 8486 keV.

The structure of the levels above 11 MeV with spins $\geq \frac{41}{2}$ has not been uniquely identified. Several possibilities exist, e.g., a $\nu(h_{11/2}g_{9/2}^{-1})$ one-neutron excitation or a $\nu(d_{5/2}^2 g_{9/2}^{-2})$ two-neutron excitation combined with the five-proton structures, or the $\nu(d_{5/2}g_{9/2}^{-1})$ excitation coupled to six-particle–one-hole proton structures with the proton hole in the $f_{5/2}$ or $p_{3/2}$ shell. The experimental data for these highest levels is not sufficiently informative to allow a choice between the different alternatives.

B. Discussion of levels in ^{94}Ru

The experimental level scheme is given in Fig. 5. The levels with probable configuration assignments are reproduced in Fig. 13. Those levels which are interpreted as pure proton states are compared with the calculated spectrum of Sinatkas *et al.* [14] in Fig. 12. The energy agreement is very good for the even-parity states up to 12_1^+ with the main configuration $\pi(p_{1/2}^2 g_{9/2}^4)$. The odd-parity states up to 13_1^- with the main configuration $\pi(p_{1/2}g_{9/2}^5)$ and the 12_2^+ state of the $\pi(g_{9/2}^6)$ configuration are systematically calculated too high compared to

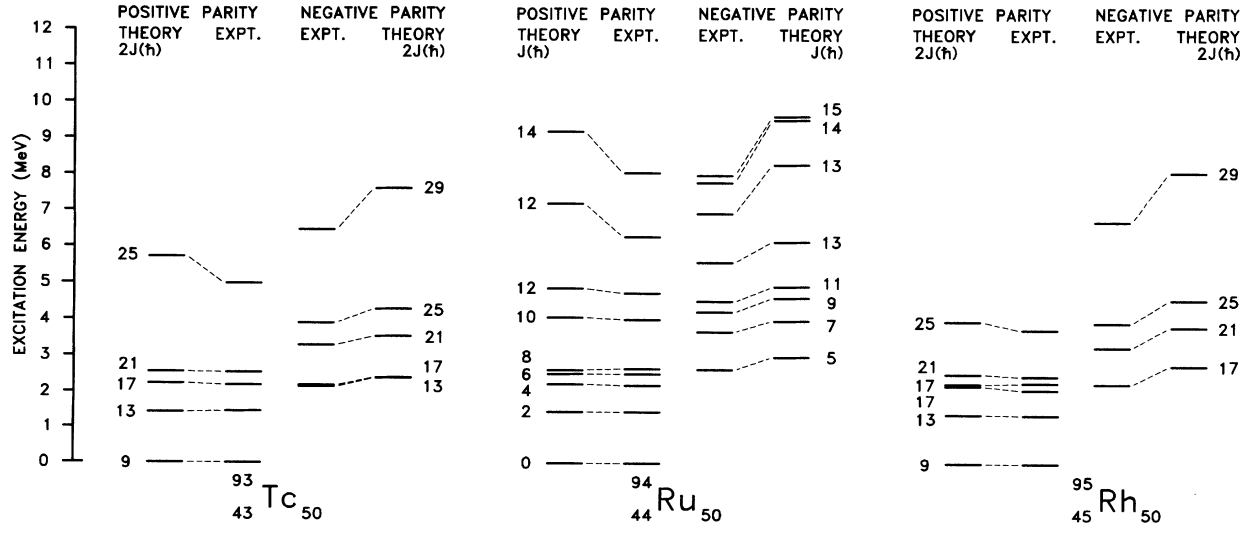

FIG. 12. Comparison between theoretically predicted (Sinatkas *et al.* [14]) and experimentally established yrast levels in ^{93}Tc, ^{94}Ru, and ^{95}Rh. Mainly yrast levels thought to be described by a p, $f_{5/2}$, $g_{9/2}$ configuration are shown.

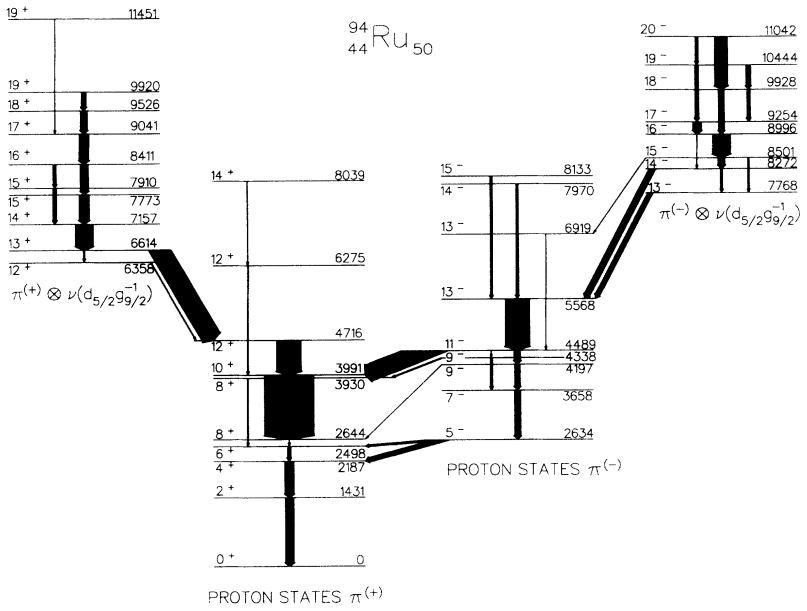

FIG. 13. Structural scheme for ^{94}Ru, showing a representative selection of levels and transitions.

the $\pi(p_{1/2}^2 g_{9/2}^4)$ states. This situation resembles closely the analogous comparison for ^{93}Tc, and is understood as a consequence of the too large spacing between the $p_{1/2}$ and $g_{9/2}$ shells used in the calculation. The experimental levels at 6919 keV (13^-), 7970 keV (14^-), 8133 keV (15^-), and 8039 keV (14^+) are tentatively associated with the calculated states having one proton hole in the deeper $f_{5/2}$ or $p_{3/2}$ shells (Fig. 12).

The energies of the 19^+, 20^-, and 19^+ states, which are the highest-spin members of the $\pi(p_{1/2}^n g_{9/2}^{6-n})\nu(d_{5/2}g_{9/2}^{-1})$ configurations with n=2, 1, and 0, respectively, have been calculated by the same method that was used above for ^{93}Tc. The resulting calculated energies, 9960 keV (19^+), 11 010 keV (20^-), and 11 300 keV (19^+) agree well with the experimental values.

The even-parity levels in the cascade from 19^+ at 9920 keV down to 12^+ at 6358 keV are all assumed to belong to the $\pi(p_{1/2}^2 g_{9/2}^4)\nu(d_{5/2}g_{9/2}^{-1})$ configuration. The calculations by Muto *et al.* [11] reproduce the spacings between these levels fairly well, cf. Fig. 14. The complexity of the cascade on the odd-parity side down from 20^- at 11 042 keV makes the configuration identification more uncertain for some of these levels. From the decay pattern it seems probable that the levels at 11 042, 10 444, 9928, 9789, 9254, 9134, 8996, 8853, 8736, 8501, 8272, 8152, and 7768 keV belong to the $\pi(p_{1/2}g_{9/2}^5)\nu(d_{5/2}g_{9/2}^{-1})$ configuration. Also here the calculation [11] reproduces the spacings between the yrast odd-parity levels fairly well. Some of the remaining levels may belong to the $\pi(p_{1/2}^2 g_{9/2}^4)\nu(h_{11/2}g_{9/2}^{-1})$ configuration.

A fairly rich spectrum has been found above the 19^+ and 20^- levels. The experimental information is not sufficient to identify the configurations for most of the states, in particular, when the spin-parity assignments are uncertain. The excitation energy suggests that the 22^- level at 13 053 keV may be the maximum-spin state of the $\pi(p_{1/2}^2 g_{9/2}^4)\nu(h_{11/2}g_{9/2}^{-1})$ configuration. Similarly, the levels at 14 293 and 13 078 keV may be the 23^+ and 21^+ states of the $\pi(p_{1/2}g_{9/2}^5)\nu(h_{11/2}g_{9/2}^{-1})$ configuration. This interpretation requires that the 1240.1- and 2035.8-keV transitions have multipolarity $E1$ rather than $M1$, which is not excluded by the data. The levels with spin >22 probably involve excitations of two neutrons across the N=50 gap.

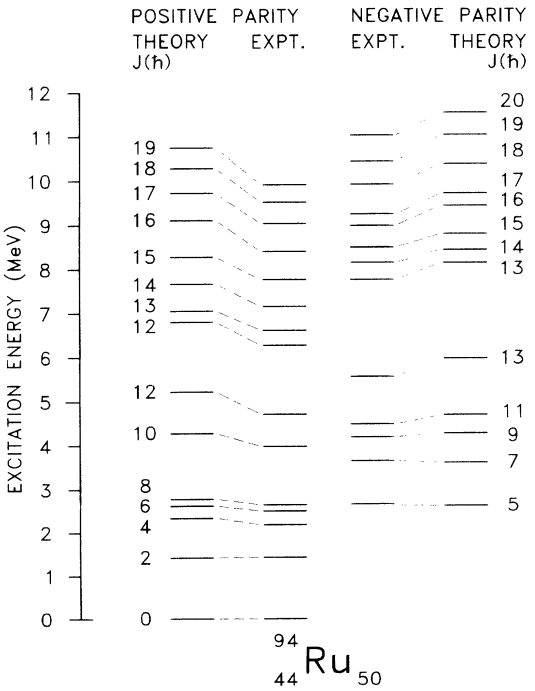

FIG. 14. Comparison between theoretically predicted (Muto *et al.* [11]) and experimentally established yrast levels in ^{94}Ru. The model [11] used includes neutron core excitation across the N=50 shell.

C. Discussion of levels in ^{95}Rh

The experimental level scheme is given in Fig. 8 and the structural interpretation of the levels in Fig. 15. The lower levels up to 4 MeV, for which the angular momentum is carried by the protons, are compared with the calculations of Sinatkas *et al.* [14] in Fig. 12. In analogy with the ^{93}Tc and ^{94}Ru cases, the calculation reproduces very well the relative energies within the group $\frac{9}{2}^+$, $\frac{13}{2}^+$, $\frac{17}{2}^+_1$, $\frac{17}{2}^+_2$, $\frac{21}{2}^+$, $\frac{25}{2}^+$ of the $\pi(p^2_{1/2}g^5_{9/2})$ configuration, and the group $\frac{17}{2}^-$, $\frac{21}{2}^-$, $\frac{25}{2}^-$ of the $\pi(p_{1/2}g^6_{9/2})$ configuration, although the two groups are shifted relative to each other.

The levels with a neutron $\nu(d_{5/2}g^{-1}_{9/2})$ excitation coupled to the protons occur between 4 and 10 MeV. The energies of the $\frac{39}{2}^+$ and $\frac{39}{2}^-$ states, which are the highest-spin members of the $\pi(p^n_{1/2}g^{7-n}_{9/2})\nu(d_{5/2}g^{-1}_{9/2})$ configurations with $n = 2$ and 1, have been calculated at 8910 keV ($\frac{39}{2}^+$) and 9300 keV ($\frac{39}{2}^-$). The agreement with the experimental energies is very good, even to the extent that the deviations go in the same directions as for the equivalent states in ^{93}Tc and ^{94}Ru. Based on these observations we can predict the energies for the same type of neutron-excited states in the neighboring $N=50$ isotones ^{92}Mo and ^{96}Pd: $E(15^+,{}^{92}\text{Mo})=8110$ keV, $E(18^-,{}^{92}\text{Mo})=10\,140$ keV, and $E(19^+,{}^{96}\text{Pd})=9670$ keV, $E(18^-,{}^{96}\text{Pd})=9830$ keV. None of these levels have so far been identified in experiments.

The even-parity levels in the cascade from $\frac{39}{2}^+$ at 8874 keV down to $\frac{21}{2}^+$ at 4241 keV are all assumed to belong to the $\pi(p^2_{1/2}g^5_{9/2})\nu(d_{5/2}g^{-1}_{9/2})$ configuration. On the odd-parity side the cascade down to $\frac{31}{2}^-$ at 7511 keV can be understood as transitions within the $\pi(p_{1/2}g^6_{9/2})\nu(d_{5/2}g^{-1}_{9/2})$ configuration. The interpretation of the four levels at 7064, 6698, 6585, and 6404 keV is more problematic. The strong 1147.2-keV transition and the low-energy 114.1- and 293.8-keV transitions indicate that the three levels at 6698, 6585, and 6404 keV also belong to this same configuration. However, in this case the $\frac{29}{2}^-$ level at 7064 keV cannot be interpreted as the maximum-spin state of the $\pi(f^{-1}_{5/2}p^2_{1/2}g^6_{9/2})$ configuration, since the intensity ratio $I_\gamma(447.5\text{ keV})/I_\gamma(813.3\text{ keV})$ is much too large, and also because of the absence of an $E2$ transition to the 3908-keV level. An alternative interpretation is suggested in Fig. 15, changing the roles of the $\frac{29}{2}^-$ states. It is also possible that both $\frac{29}{2}^-$ states are neutron excitations.

The levels above 10 MeV cannot be given unique configuration assignments. One may expect to find states at these energies involving the one-neutron excitation $\nu(h_{11/2}g^{-1}_{9/2})$, or the two-neutron excitation $\nu(d^2_{5/2}g^{-2}_{9/2})$, or the one-neutron excitation $\nu(d_{5/2}g^{-1}_{9/2})$ multiplying a proton configuration with one hole in the deeper $\pi f_{5/2}$ or $\pi p_{3/2}$ shells. The $45/2^\pm$ maximum-spin states of the first kind should occur around 12 MeV. These yrast states have apparently not been produced with sufficient intensity in the present experiment.

V. SUMMARY

We have studied the $N=50$ isotones ^{93}Tc, ^{94}Ru, and ^{95}Rh produced in the ^{40}Ca+^{58}Ni fusion reaction. We used the multidetector system NORDBALL at NBI, Risø, with 15 BGO-shielded HPGe γ-ray detectors, a 4π Si ball consisting of 21 Si detectors, and 11 liquid scintillator neutron detectors.

The level schemes of all three nuclei have been extended to spin values of 20 and higher. A large number of new levels have been identified.

We have compared our level schemes with the recent shell-model calculations of Sinatkas *et al.* [14]. For the low-lying states with $I \leq 13$, which are dominated by configurations with protons within the restricted $p_{1/2}$, $g_{9/2}$ basis, the calculated energies agree very well with the

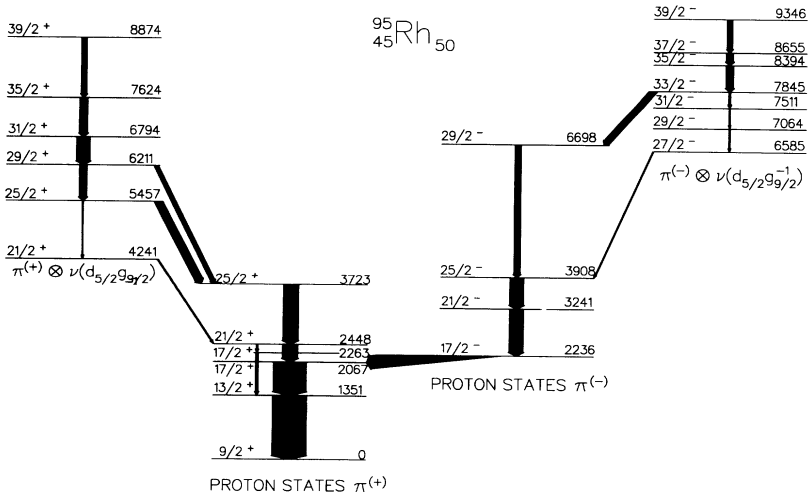

FIG. 15. Structural scheme for ^{95}Rh, showing a representative selection of levels and transitions.

TABLE V. Energy (MeV) needed to form a $\nu(d_{5/2}g_{9/2}^{-1})$ particle-hole pair of maximal spin (7), and then align in with $\pi(p_{1/2}^{n}g_{9/2}^{m-n})$ configurations (m = 3–6, and n=2 or 1, respectively) of maximal spin. Values from Ref. [24] (N=49), and from the present work. The level energies on which the differences are based are also given. Parentheses around a value indicate that the spin of the upper level is possible but not ascertained.

Positive parity			Negative parity	
		N=49		
^{93}Ru	(5.54)	(=10.88−5.34)	5.98	(=11.95−5.97)
^{94}Rh	5.60	(=10.10−4.50)	6.03	(=10.43−4.40)
^{95}Pd	(5.67)	(=10.35−4.68)		
Mean	5.60		6.00	
Range	±0.07		±0.03	
		N=50		
^{93}Tc	5.28	(=7.81−2.53)	5.53	(=9.42−3.89)
^{94}Ru	5.20	(=9.92−4.72)	5.47	(=11.04−5.57)
^{95}Rh	5.15	(=8.87−3.72)	5.44	(=9.35−3.91)
Mean	5.21		5.48	
Range	±0.07		±0.05	

experimental values. We have noticed systematic shifts between the groups of states with 2, 1, or 0 protons in the $p_{1/2}$ shell, which we attribute to a too large spacing between the $p_{1/2}$ and $g_{9/2}$ single-particle energies used in the calculations.

The main new result of our work is the identification of many higher levels with spins above the values that can be reached in the restricted shell-model basis. Most of the new levels correspond to configurations with a neutron particle-hole excitation $\nu(d_{5/2}g_{9/2}^{-1})$ coupled to proton states $\pi(p_{1/2},g_{9/2})^m$ with m=5, 6, or 7. States with the maximum neutron spin 7 aligned with the maximum proton spin from the $\pi(p_{1/2},g_{9/2})^m$ configurations have been observed in all three nuclei for both parities. The energy differences between these aligned neutron-excited states and the respective proton basis states are displayed in Table V. The values are remarkably constant, 5.21(7) MeV for the positive-parity levels and 5.48(5) MeV for the negative-parity levels. For levels of this type in the region $J \approx$13–20 the calculations of Muto *et al.* [11] are generally in good agreement with our ^{94}Ru results.

Above about 10 MeV we have observed a number of levels with even higher spins. There are several possible configuration assignments for these levels, but the experimental information is in general not detailed enough to give preference to one or the other.

ACKNOWLEDGMENTS

The authors are grateful to the staff of the Niels Bohr Institut, Risø, for their hospitality and for providing beams and technical support. We are especially indebted to Jörn Westergaard for operating the NBI Tandem van de Graaff and booster accelerator system. The interest in our work and the support from Dr. G. Sletten is greatly appreciated. We are very thankful to Dr. L. D. Skouras, Athens, for sending us the results of shell-model calculations prior to publication. We also want to thank Dr. D. C. Radford for giving us access to his very useful computer program ESCL8R. The support from the Swedish Natural Science Research Council (NFR), the Danish Natural Science Research Council (SNF), and the Japanese Government is greatly appreciated.

[1] I. Talmi and I. Unna, Nucl. Phys **19**, 225 (1960).
[2] S. Cohen, R. D. Lawson, M. H. Macfarlane, and M. Soda, Phys. Lett. **10**, 195 (1964).
[3] N. Auerbach and I. Talmi, Nucl. Phys. **64**, 458 (1965).
[4] J. Vervier, Nucl. Phys. **75**, 17 (1965).
[5] J. B. Ball, J. B. McGrory, R. L. Auble, and K. H. Bhatt, Phys. Lett. **29B**, 182 (1969).
[6] D. H. Gloeckner, M. H. Macfarlane, R. D. Lawson, and F. J. D. Serduke, Phys. Lett. **40B**, 597 (1972).
[7] J. B. Ball, J. B. McGrory, and J. S. Larsen, Phys. Lett. **41B**, 581 (1972).
[8] D. H Gloeckner and F. J. D. Serduke, Nucl. Phys. **A220**, 477 (1974).
[9] H. C. Chiang, M. C. Wang, and C. S. Han, J. Phys. G **6**, 345 (1980).
[10] A. Amusa and R. D. Lawson, Z. Phys. A **307**, 333 (1982).
[11] K. Muto, T. Shimano, and H. Horie, Phys. Lett. **135B**, 349 (1984).
[12] J. Blomqvist and L. Rydström, Phys. Scr. **31**, 31 (1985).
[13] X. Ji and B. H. Wildenthal, Phys. Rev. C **37**, 1256 (1988).
[14] J. Sinatkas, L. D. Skouras, D. Strottman, and J. D. Vergados, J. Phys. G **18**, 1377 (1992).
[15] E. Nolte, G. Korschinek, and U. Heim, Z. Phys. A **298**, 191 (1980).
[16] W. F. Piel, G. Scharff-Goldhaber, C. J. Lister, and B. J. Varley, Phys. Rev. C **28**, 209 (1983).
[17] S. E. Arnell, T. Kuroyanagi, S. Mitarai, J. Nyberg, H. A. Roth, and Ö. Skeppstedt, the NORDBALL system adopted for spectroscopy of nuclei far from stability, *Proceedings of the Nuclear Physics in the Nineties*, Oak Ridge, Tennessee (Oak Ridge National Laboratory, Oak Ridge, Tennessee, 1990), Vol. 1, p. 214.
[18] M. Grecescu, A. Nilsson, and L. Harms-Ringdahl, Nucl. Phys. **A212**, 429 (1973).
[19] B. A. Brown, D. B. Fossan, P. M. S. Lesser, and A. R. Poletti, Phys. Rev. C **13**, 1194 (1976).
[20] S. S. Ghugre, S. B. Patel, M. Gupta, R. K. Bhowmik, and J. A. Sheikh, Phys. Rev. C **47**, 87 (1993).
[21] A. Nilsson and M. Grecescu, Nucl. Phys. **A212**, 448 (1973).
[22] F. Pühlhofer, Nucl. Phys. **A280**, 267 (1977).
[23] B. Herskind, Nucl. Phys. **A447**, 395c (1985).
[24] S. E. Arnell, D. Foltescu, H. A. Roth, Ö. Skeppstedt, J. Blomqvist, A. Nilsson, T. Kuroyanagi, S. Mitarai, and J. Nyberg, Phys. Rev. C **49**, 51 (1994).

[25] T. Kuroyanagi, S. Mitarai, S. Suematsu, B. J. Min, H. Tomura, J. Mukai, T. T. Maeda, R. Nakatani, G. Sletten, J. Nyberg, and D. Jerrestam, Nucl. Instrum. Methods Phys. Res. Sect. A **316**, 289 (1992).
[26] S. E. Arnell, H. A. Roth, Ö. Skeppstedt, J. Bialkowski, M. Moszynski, D. Wolski, and J. Nyberg, Nucl. Instrum. Methods Phys. Res. Sect. A **300**, 301 (1991).
[27] D. C. Radford, private communication; D. C. Radford *et al.*, Nucl. Phys. **A545**, 665 (1992).
[28] H. Sievers, Nucl. Data Sheets **54**, 119 (1988).
[29] W. D. Schneider, K. H. Gonsior, and C. Günther, Nucl. Phys. **A249**, 103 (1975).
[30] T. W. Burrows, Nucl. Data Sheets **68**, 635 (1993).